Research Square

Preprints are preliminary reports that have not undergone peer review.
They should not be considered conclusive, used to inform clinical practice,
or referenced by the media as validated information.

dTF-FCU1-Armed Vaccinia Virus Synergizes with the 5-FC Prodrug to Induce Immunogenic Cell Death and Remodel Immunosuppressive Tumor Microenvironment

Fei Guo

guofei@ipb.pumc.edu.cn

Chinese Academy of Medical Sciences and Peking Union Medical College https://orcid.org/0000-0003-3500-1006

Liming Wang
Yu Huang
Shan Mei
Fei Zhao
Lingwa Wang
Zhao Gao
Jiaxun Wang
Ziyue Kong
Maozhong Wang
Siqi Rong
Rurong He
Yueyue Shi
WenKai Guo
Jugao Fang
Bin Ai
Fengwen Xu

Article

Keywords: oncolytic viruses, vaccinia virus, prodrug, cancer immunotherapy, tumor microenvironment

Posted Date: August 27th, 2026

DOI: https://doi.org/10.21203/rs.3.rs-10701717/v1

License: This work is licensed under a Creative Commons Attribution 4.0 International License.
Read Full License

Additional Declarations: There is **NO** conflict of interest to disclose.

Abstract

Oncolytic virotherapy (OVT) serves as a powerful platform for targeted prodrug delivery. Vaccinia virus (VACV) serves as an attractive oncolytic vector due to its favorable safety profile, ease of genetic modification, and inherent tumor selectivity. We engineered an oncolytic vaccinia virus, dTF-FCU1, by inserting the prodrug-converting enzyme gene *FCU1* and deleting the *J2R* and *F4L* genes to enhance tumor selectivity. When combined with the prodrug 5-Fluorocytosine, dTF-FCU1 induced pronounced DNA damage and immunogenic cell death in cancer cells. In murine cancer model, this combination significantly suppressed tumor growth, enhanced antitumor immunity by promoting cytotoxic $CD8^+$ T-cell infiltration, and alleviating immune resistance by reducing Tregs, exhausted T cells and M2-type macrophages, thus reshaping the tumor immune microenvironment. Our study demonstrates strong selectivity and high efficacy of the dTF-FCU1/5-FC strategy, supporting its further development into a cancer treatment.

Introduction

Oncolytic viruses are a class of therapeutic agents that can selectively infect and replicate within tumor cells, ultimately lysing cancer cells and eliciting systemic anti-tumor immunity. Due to their unique mechanism of action in remodeling the tumor microenvironment (TME), they have become a promising novel tool in tumor immunotherapy[1]. Diverse viruses have oncolytic property, including DNA viruses (e.g., adenovirus (Ad), vaccinia virus (VACV), herpesvirus) and RNA viruses (e.g., reovirus, measles virus, New Castle disease virus (NDV), vesicular stomatitis virus (VSV)). DNA oncolytic viruses often offer a few advantages such as their large genome size, high genetic stability, and robust replication capacity[2].

Oncolytic VACV is one of the most widely used platforms, featuring a large genomic capacity and a well-established safety profile. Most oncolytic VACVs reported to date are mutated in the *J2R* gene [3,4]. However, *J2R* deletion alone is insufficient to confer high selectivity. In previous clinical trials using oncolytic *J2R*-deleted VACVs, approximately 10%–20% of patients developed vaccinia-associated pustular skin lesions[4]. Therefore, further optimization of the VV-dTK (thymidine kinase) backbone is required to improve tumor selectivity. Since DNA virus replication requires deoxynucleoside triphosphates (dNTPs), further deletion of genes encoding ribonucleotide reductase (RR) which is required for dNTP production becomes a feasible strategy. RR deletion helps to restrict DNA viruses to replicate in rapidly proliferating tumor cells with high dNTP pools, thereby enhancing tumor selectivity[5–9]. VACV *I4L* and *F4L* genes encode homologs of the large (RRM1) and small (RRM2) subunits of RR, respectively[10,11]. Studies have shown that dual deletion of *J2R* together with *I4L* or *F4L* can generate viral strains with high selectivity for a variety of tumor cells, including hepatocellular carcinoma (HCC) and bladder cancer[8,12].

To enhance the tumor-killing efficacy of oncolytic viruses (OVs), the FCU1 gene from fusion yeast was armed. This gene encodes a bifunctional chimeric protein that catalyzes the conversion of non-toxic 5-

fluorocytosine (5-FC) into the toxic metabolites 5-fluorouracil (5-FU) and 5-fluorouracil-monophosphate (5-FUMP). 5-FUMP interferes with DNA and RNA synthesis[4,13], causes double-stranded DNA breaks (DSBs)[14] and onset of apoptosis[15–17]. Utilizing the tumor-selective replication property of oncolytic VACV, the prodrug-converting enzyme (FCU1) is expressed specifically at the tumor site, converting prodrug 5-FC into active 5-FU, thereby achieving targeted tumor killing. This approach enhances efficacy through local drug enrichment and the “bystander effect” at the tumor site, while substantially reducing the systemic toxicity associated with conventional chemotherapy[4].

The antitumor mechanism of OVs involves the replication of viruses in tumor cells, which kills the tumor cells directly, or the lysis of tumor cells, which triggers the release of a large number of tumor antigens and danger signals, thereby resulting in immunogenic cell death (ICD). ICD constitutes a prominent pathway for activating the immune system against cancer, which in turn determines the long-term success of anticancer therapies[18]. Many recent studies demonstrate that a variety of OVs, such as oAds, oncolytic herpes simplex virus, oncolytic VACV, oncolytic NDV, and oncolytic measles virus, could trigger immunogenic tumor cell death[19]. As mentioned above, FCU1/5-FC can induce DSBs and apoptosis in tumor cells. Nonetheless, whether FCU1/5-FC can further enhance VACV-induced immunogenic tumor cell death has not been reported.

Drawing on the principles outlined above, we initially compared the effects of *I4L* and *F4L* on the tumor selectivity of dTK-FCU1 and observed that deletion of *F4L* better supported the selective replication of dTK-FCU1 in tumor cells, as well as for the selective killing of tumor cells in combination with prodrug 5-FC. Further investigation into the antitumor mechanism revealed that the dTF-FCU1/5-FC combination elicited substantial genomic damage and robust ICD. In murine models, the dTF-FCU1/5-FC combination not only potently activated cytotoxic T lymphocyte (CTL) differentiation and effector T-cell expansion, but also alleviated immunosuppressive barriers, including T-cell exhaustion and tumor-associated macrophage (TAM). This therapeutic approach presents a favorable safety profile, and drives profound remodeling of the tumor immune microenvironment, thereby eliminates tumor cells.

Materials and Methods

Cell culture

The human lung cancer cell line A549 (ATCC, CCL185), human hepatocarcinoma cell lines Huh-7 (Procell, CL-0120) and HepG2 (ATCC, HB-8065), human skin fibroblast cell line HSF were maintained in DMEM supplemented with 10% FBS + 1% P/S. The human normal hepatocyte cell line THLE-2 (ATCC, CRL-2706) was cultured in RPMI-1640 purchased from Procell (PM150110B). The murine lung cancer cell line LLC (ATCC, CRL-1642) was cultured in 1640 purchased from Procell (CM-0141). All cells were maintained at 37℃ with 5% CO_2. 5-FC was purchased from Aladdin (2022-85-7).

Plasmids

The shuttle plasmid pJSA-TK contained the vaccina virus early/late promoter P7.5 and late promoter P11, surrounded by the flanking sequences of VACV *J2R* gene. Similarly, the shuttle plasmid pJSA-F4L and pJSA-I4L both contained promoter P7.5 and late promoter P11, surrounded by the flanking sequences of VACV *F4L* or VACV *I4L* gene respectively. To obtain shuttle vector pJSA-FCU1, the *FCU1* gene was cloned from plasmid pUpstream2Lox purchased from Addgene (#164573). The 5' primer (5'-CAGTGACGGATCCCCGGGCCATGGATGGTGACAGGGGGAATGGCAAGCAAGTGGGATCA-3') was designed to introduce a NocI site for cloning. The 3' primer (5'-CACTTTCTACGTCGACGCGGCCGCTTAAACACAGTAGTATCT-3') introduced a NotI site. Then the FCU1 cDNA was inserted downstream of the promoter P7.5 in the pJSA plasmid through homologous recombination.

Virus preparation

All recombinant viruses were derived from parental vaccinia virus Tiantan strain. Briefly, the J2R-deleted VV, △F4L-VV or △I4L -VV was rescued with shuttle plasmid pJSA-TK or pJSA-FCU1 by homologous recombination. Recombinant VAVCs were purified by plaque assay. After five rounds of plaque purification, recombinant regions were confirmed by PCR and DNA sequencing. Purified recombinant viruses were amplified by infecting Vero cells and quantified by plaque assay. Primers used were as follows:

J1R-J3R-F: 5'-CGATGTTCTTCGCAGATGATG-3';

J1R-J3R-R: 5'-CTTTGTTACGGACGATCTTATTAAGGTAGT-3';

F3L-F5L-F: 5'-ATTGCCTCCTATGGCATCAAT-3';

F3L-F5L-R: 5'-GAACCCATCCTTGCACCAAAT-3';

I3L-I5L-F: 5'-GCAGTAGGTCTTGGTGAAGTTTCA-3';

I3L-I5L-R: 5'-ATCGAGCCGTAACGATTTTCAAAT-3'.

In vitro FCU1 enzymatic assay

Spectrophotometry was used based on the method described by Singh[20]. CD-UPRT activity was determined by measuring the relative changes in substrate concentration using the optical absorbance spectrum of 5-FC (peak at 285–290 nm). 1.5⍰10^5 A549 cells were cultured in 12-well plates and infected with VACV at MOI = 1. At specified time post-infection, the culture medium was discarded, replaced with 0.9% NaCl. Cells were lysed by one freeze-thaw cycle. Whole cell lysates were incubated at 37 ℃ with 5-FC at a final concentration of 1.5 mM for 48 h. After centrifugation at 6,000 g for 5 min at 4 ℃, the supernatant was transferred into a 96-well plate and the absorbance at 285 nm was determined using an enzyme-linked immunosorbent assay reader.

In vitro viral replication

The virus yield was used to evaluate the specificity of virus infection in tumor cells and normal cells. Two lung cancer cell lines LLC, A549, two hepatocarcinoma cells Hep G2, Huh-7, two normal cell lines HSF and THLE-2 were infected in 12-well plates (2×10^5 cells/well) with the indicated viruses at MOI = 0.005. At the indicated time points, supernatants and cells were harvested, subjected to three cycles of freeze-thaw, and the amount of progeny virus was determined with plaque assay by infecting Vero cells.

In Vitro cytotoxicity assay

The cells were cultured at a density of 1×10^4 cells/well in 96-well plates. Tumor cells and normal cells were infected by recombinant VACVs at a MOI of 0.001. 48 hours post-infection, 5-FC was added to the cell culture supernatant at a final concentration of 1mM. An equal volume of 0.9% NaCl was added to the control group. 96 hours post-infection, cell viability was assessed using the Cell Counting Kit-8 (MCE HY-K0301).

Western blotting

Western blotting
DNA damage and apoptosis were assessed by western blot. Cells were cultured in 12-well plates at a density of 2×10^5 cells/well and infected with dTF-FCU1 at an MOI of 0.001. 48 hours post-infection, a final concentration of 1mM 5-FC or an equal volume of 0.9% NaCl was added to the cell culture plate. Another 48 hours post-infection, cells were harvested for western blot analysis using the following antibodies, anti-γH2AX (Proteintech, 83307-2-RR), anti-P-CHK1 (CST, 2348S), anti-Caspase3 (CST, 9662S), anti-Cleaved-Caspase3 (CST, 9661S), anti-PARP (CST, 9542S), anti-HMGB1 (CST, 6893S), anti-HSP90 (PTG, 13171-1-AP).

Immunogenic cell death assays

HMGB1 and HSP90 were detected via western blot. Cells at a cell density of 2×10^5 cells/well were cultured in 12 well-plates and exposed to dTF-FCU1 at MOI = 0.001. Two days post-infection, a final concentration of 1mM 5-FC or an equivalent volume of 0.9% NaCl was added. Another two days post-infection, the supernatant and cells were collected separately for western blot analysis. Supernatant were centrifuged at 3000 rpm, 4℃, for 3 minutes to remove cell debris. Anti-HMGB1 and HSP90 antibodies were used for immunoblotting.

ATP and Calreticulin were measured as previously described[21]. For ATP, cells were seeded, infected in a manner similar to that in the HMGB1 experiment, and determined using luminescence-based ATP assay kit (MCE, HY-K0314) and CellTiter-Glo Luminescent Cell Viability Assay (Promega). Calreticulin exposure was assessed using flow cytometry. 5×10^5 cells/well were seeded in 12-well plates and infected with virus at the indicated MOI. 2 hours post-infection, 5-FC (1mM) or 0.9% NaCl was added. 48 hours post-

infection, cells were harvested and stained with allophycocyanin (APC)-labeled anti-CRT polyclonal antibody (Proteintech, 10427-2-AP).

Animal experiments

All animal experiments were conducted in compliance with the relevant national guidelines and regulations and were approved by Institution Beijing Huilinzegu Co. Ltd's Animal Care and Use Committee (Approval No. HLZG-DWLL-2024-0602-04). Female BALB/c mice (5 ~ 6 weeks old) and female C57bl/6j (5 ~ 6 weeks old) were used in the experiments. Animals were housed in pathogen-free environment in Beijing Huilinzegu Co. Ltd and were euthanized by cervical dislocation while under anesthesia.

For the xenograft model, A549 cells were injected subcutaneously into female BALB/c nude mice at a dose of 8×10^6 cells. When the tumors reached a size of 100–150 mm^3, mice were randomly divided into three groups based on body weights and tumor volumes, each group has 5 mice. 5×10^5 PFUs dTF-FCU1 or PBS was injected intratumorally. Five days post infection, 5-FC or 0.9% NaCl was administered orally via gavage at a dosage of 100 mg per kg twice daily for two weeks. Tumor size was measured twice a week with calipers. Tumor volume (mm^3) was calculated as (length×$width^2$)/2. Mouse weight was measured at the same frequency as tumor measurements. Mice were monitored every three days and euthanized if tumor diameter exceeded 20mm or if body weight loss exceeded 20%.

For syngeneic model, female C57bl/6j mice were injected subcutaneously with 1×10^6 LLC cells. Once the average tumor size reached around 150 mm^3, the mice were randomly divided into three groups according to their body weights and tumor volumes, each group has 13 mice. Two cycles of dTF-FCU1/5-FC were administered. 1×10^7 PFUs dTF-FCU1 or PBS was injected intratumorally, and 5-FC or 0.9% NaCl was given on the next day for a total of 5 days, at the same doses and frequency as in the nude mouse experiment. After completing the first 5-FC treatment cycle, dTF-FCU1 was injected again at 1×10^7 PFUs, followed by another 5-day course of 5-FC. After two rounds of dTF-FCU1/5-FC treatment, on the following day, tumors and spleens of 6 mice were harvested from each group randomly, and the rest were monitored for changes in tumor size and body weight. Tumor size and body weight were measured twice a week. Mice were monitored every three days and euthanized if tumor diameter exceeded 20mm or if body weight loss exceeded 20%.

Immunohistochemistry and immunofluorescence

Tumor tissues were fixed in 4% formaldehyde and embedded in paraffin. For detection of ICD, paraffin sections were incubated for 1.5 h at room temperature with the primary antibodies against HSP90 (Proteintech, 13171-1-AP). Then, horseradish peroxidase (HRP) -conjugated dextran polymer goat anti-rabbit IgG (Dako) was used and the HRP activity was visualized by DAB Substrate Chromogen.

To detect CD8, paraffin sections were incubated for 1.5 h at room temperature with rabbit anti-CD8 antibody (Abcam, ab217344), and then detected using HRP-conjugated dextran polymer goat anti-rabbit IgG, followed by FITC-labeled tyramide. Tissue sections were counterstained with DAPI.

Images were recorded with Pannoramic SCAN II and analyzed using Slide Viewer software.

Flow cytometry

Fresh tumor tissues were collected and digested with Tumor Extraction Kit (130-096-730) purchased from Miltenyi Biotec. The digestate was filtered through a 70um filter membrane, then lysed with red blood cell lysis buffer to prepare single-cell suspensions.

Subsequently, the cells were sequentially stained with viability dyes, cell surface antibodies, fixed and permeabilized, and stained with intracellular antibodies.

The spleens were initially physically ground, then filtered through 70 um cell sieves. Red blood cells were removed using red blood cell lysis buffer, and prepared as single-cell suspensions. Cells were cultured in 96-well plates, stimulated with LLC peptides (FEQNTAQP (MUT1) and FEQNTAQA (MUT2)) for 8 hours[22,23]. Brefeldin A was added, and cells were incubated for an additional 8 hours, and then the cells were harvested for staining. The staining method was the same as described above for the tumor tissues.

FACS data were collected via BD FACSCelesta and analyzed via Flowjo V.10.9.0. Details of antibodies purchased from BD Bioscience were as follows, Fixable Viability Stain 780 (565388), BV786 Rat Anti-Mouse CD45 (564225), PE-Cy™7 Hamster Anti-Mouse CD3e (552774), RB705 Rat Anti-Mouse CD4 (570258), BV510 Rat Anti-Mouse CD8a (563068), PE-CF594 Hamster Anti-Mouse CD279 (PD-1) (562523), RB705 Rat Anti-CD11b (570292), BV650 Rat Anti-Mouse CD86 (564200), PE Rat Anti-Mouse CD206 (568273), BV650 Rat Anti-Mouse TNF (563943). Antibodies purchased from Biolegend were BV711™ anti-mouse CD366 (Tim-3) (119727), BV421™ anti-mouse FOXP3 (126419), BV605™ anti-human/mouse Granzyme B (396434).

Statistical analysis

Data were analyzed for statistical significance using Prism software (GraphPad). Significance was tested using one-way ANOVA or two-way ANOVA as indicated. Data for animal survival curves were analyzed by Mantel-Cox test. Data are expressed as variance ± standard error of the mean or standard deviation (SD). $P < 0.05$ was considered to be statistically significant.

Results

dTF-FCU1 exhibits high tumor-selectivity for its replication

First, the *FCU1* gene was inserted into the TK locus of VACV via homologous recombination, generating the recombinant virus dTK-FCU1 (Fig. 1A). Then the large and small subunits of RRM2 (encoded by *I4L* and *F4L*) were individually deleted, to develop a safer oncolytic VACV (Fig. 1A). The *J2R*, *F4L*, and *I4L* regions of the recombinant viruses were amplified and sequenced with specific primers (Fig. 1B). FCU1 expression (approximately 40 kDa) was confirmed by western blotting (Fig. 1C).

To assess the activity of FCU1, the cytidine/deoxycytidine uridine phosphoribosyltransferase (CD-UPRTase) activity of VACV-expressed FCU1 was determined using a photometric assay that measures the conversion of 5-FC. As the substrate prodrug 5-FC gradually was converted to intermediate product 5-FU, the concentration of 5-FC decreased, leading to a reduction in its absorbance value at a wavelength of 285nm. In cells infected with dTK-FCU1, dTF-FCU1, or dTI-FCU1, 5-FC levels decreased over time, whereas no change was observed in dTK-infected cells, confirming the activity of FCU1 (Fig. 1D).

To compare which RR subunit confers greater tumor-selective viral replication, recombinant viruses were used to infect human normal skin fibroblasts (HSF) and two lung cancer cell lines (human A549 and murine LLC). In the HSF, dTI-FCU1 achieved a viral titer comparable to those of VV and dTK-FCU1 at 48 hours post-infection, measuring approximately at 3×10^5 PFU/mL, 8×10^5 and 6×10^5 PFU/mL, respectively (Fig. 1E). In contrast, the replication of dTF-FCU1 was significantly attenuated, with a titer of 1.6×10^4 PFU/mL, approximately 55-fold lower than that of VV, 40-fold lower than that of dTK-FCU1 (Fig. 1E). This trend sustained across the time course, indicating that the TK/F4L deletion imposed a more stringent restriction on viral replication in normal cells than the TK/I4L deletion. However, the attenuated replication of dTF-FCU1 was substantially rescued in the lung tumor cell line A549. The replication kinetics and titer of dTF-FCU1 are similar to those of VV and dTK-FCU1 (4.1×10^5 PFU/mL, 1.1×10^6 PFU/mL and 1.1×10^6 PFU/mL, respectively), indicating that the TK/F4L deletion had minimal impact on viral replication in tumor cells (Fig. 1E). Similar results were obtained in LLC cells, although the overall replication levels of VACV were lower due to the species-specific restriction (Fig. 1E).

A similar selectivity profile was also observed in hepatocytes. In the normal human liver cell line THLE-2, the replication of dTF-FCU1 was severely impaired, yielding titers that were approximately 11-fold lower than that of VV at 48 hours post-infection, and 5-fold lower than those of dTK-FCU1 and dTI-FCU1. In contrast, the replication defect of dTF-FCU1 was rescued in the hepatocellular carcinoma cell lines (HepG2 and Huh-7). In those tumor cells, the titer of dTF-FCU1 was only 5- to 6-fold lower than that of VV. The replication level of dTF-FCU1 was comparable to that of dTK-FCU1 and dTI-FCU1 (HepG2) (Figure S1A).

Collectively, these data demonstrate severe attenuation of dTF-FCU1 in normal cells, but robust replication in tumor cells, which supports greater tumor-selective replication of dTF-FCU1 than dTI-FCU1.

The combination of dTF-FCU1 and 5-FC further enhances the specific killing of tumor cells

To evaluate the synergistic cytotoxicity of dTF-FCU1 when combined with 5-FC, we assessed cell viability using the Cell Counting Kit-8 (CCK8) assay. Across all cell lines tested, the combination treatment (dTF-FCU1/5-FC) reduced cell viability more than dTF-FCU1 alone, with the most pronounced effects observed in tumor cells. In A549 and LLC lung tumor cells, dTF-FCU1/5-FC decreased cell viability by 35% and 60%, respectively (Fig. 2A), and by 45% in HepG2 hepatocellular carcinoma cells (Figure S2A). In contrast, the reduction by dTF-FCU1/5-FC in non-tumor cells was notably weaker, with viability declining by 20% in HSF cells (Fig. 2A). These results indicate that the combination of dTF-FCU1 and 5-FC causes much stronger cytotoxicity in tumor cells than in non-tumor cells. Consistently, the greater tumor selectivity of dTF-FCU1 over dTI-FCU1 was confirmed by higher HSF survival rates following the dTF-FCU1/5-FC treatment than the dTI-FCU1/5-FC treatment (65% vs. 40%) (Fig. 2A).

Both VACV infection and 5-FC metabolites induce DSBs[14,24], which in turn triggers apoptosis[15–17]. We observed that dTF-FCU1 infection activated DNA damage (phosphorylation of H2AX and CHK1) and cell apoptosis (cleaved of Caspase3 and PARP), and these effects were further enhanced when combined with 5-FC, especially in A549 and LLC cells (Fig. 2B-2C). Activation of DNA damage and apoptosis were also observed in HepG2 and Huh-7 with the dTF-FCU1/5-FC treatment (Figure S2B-2C). These results suggest that the cytotoxicity of dTF-FCU1/5-FC on tumors cells is a result of not only direct oncolysis but also the induction of DNA damage and apoptosis.

Subsequently, the *in vivo* oncolytic effects of dTF-FCU1/5-FC were tested in Balb/c nude mice with subcutaneously implanted A549 cells (Fig. 2D). dTF-FCU1 was administered as a single intratumoral injection of 5□10^5 PFU, and oral 5-FC (twice daily) was initiated five days post-injection for two weeks. Throughout the experiments, no significant changes in body weight were observed in the treated groups compared with the PBS control (Fig. 2F), indicating favorable safety profiles for both dTF-FCU1 monotherapy and its combination with 5-FC at the administered doses. Compared with the PBS control, dTF-FCU1 alone significantly slowed tumor growth rate (Fig. 2E, 2G), and combination with 5-FC further enhanced this antitumor effect (Fig. 2E, 2G). This indicates that dTF-FCU1/5-FC exhibits potent anticancer effect with a favorable safety profile.

Collectively, these data demonstrate that the dTF-FCU1/5-FC combination treatment induces genomic damage, activates apoptotic pathways in tumor cells, and exhibits significant antitumor activity.

dTF-FCU1 and 5-FC in combination induces synergistic ICD in tumor cells.

ICD is essential for the establishment of long-term anti-tumor immunity[25]. Cell death is divided into ICD and non-ICD, which is based on changes in cell surface markers and the release of soluble mediators, including cell surface calreticulin (CRT), high mobility group box-1 protein (HMGB1), ATP, heat shock proteins 70 (HSP70) and HSP90. These signals are recognized by immune cells, and trigger antitumor immune responses[26]. Given the enhanced cytotoxicity observed with the dTF-FCU1/5-FC treatment, we next assessed ICD status following dTF-FCU1 infection alone or in combination with 5-FC. First, assessment of CRT exposure revealed that dTF-FCU1 monotherapy elicited a moderate increase in CRT,

whereas the addition of 5-FC significantly increased the number of CRT-positive cells, particularly in A549 and LLC tumor cells (Fig. 3A). In line with this observation, dTF-FCU1 infection promoted the release of ATP, HMGB1, and HSP90 into culture supernatants. Notably, these effects were further augmented upon combination with 5-FC (Fig. 3B-3C). Importantly, this enhancement of ICD hallmarks was consistently more pronounced in tumor cells (A549 and LLC) than in normal HSF cells, underscoring the tumor-selective nature of the response (Fig. 3A-3C). Similar results were obtained in hepatocellular carcinoma cells, where the dTF-FCU1/5-FC combination significantly upregulated CRT, ATP, HMGB1, and HSP90 levels in both Huh-7 and HepG2 cells compared to THLE-2 cells (Figure S3A-3C).

Together, these data demonstrate that the combination of dTF-FCU1 with 5-FC induces stronger ICD specifically within tumor cells.

dTF-FCU1 in combination with 5-FC generates strong anti-tumor effect in immunocompetent mice

The immune system plays a crucial role in anti-tumor response. The antitumor effect of dTF-FCU1/5-FC combination therapy was demonstrated in the immunodeficient tumor-bearing mice. Next, we measured the oncolytic effects of dTF-FCU1/5-FC in a syngeneic mouse lung cancer model which was established with C57BL/6 immunocompetent mice bearing subcutaneous LLC tumors.

Two cycles of dTF-FCU1/5-FC were administered. A single intratumoral injection of dTF-FCU1 (1□10^7 PFUs) was performed, followed by oral administration of 5-FC (or PBS) for five consecutive days starting the day after viral infection. At the end of the first 5-FC regimen, a second identical dose of dTF-FCU1 was injected into tumor sites and 5-FC was administered on the second day for 5 days (Fig. 4A). No weight loss was observed in dTF-FCU1 and dTF-FCU1/5-FC treated mice, indicating favorable safety profiles (Fig. 4B). Compared to the PBS control group, dTF-FCU1 alone suppressed tumor growth significantly and improved survival, with mortality resulting from excessive tumor burden (Fig. 4C-4F). When dTF-FCU1 was combined with 5-FC, tumor growth was further suppressed and survival time was extended (Fig. 4C-4F). These data suggest that dTF-FCU1 and 5-FC in combination synergistically enhance the therapeutic efficacy against tumor while maintaining a favorable safety profile in immunocompetent mice.

dTF-FCU1 in combination with 5-FC improves the tumor immune environment by boosting effector T cells and reducing inhibitory T cells

OVs can convert a “cold” TME into a “hot” one, which is crucial for counteracting tumor immune evasion[27]. Given that the dTF-FCU1/5-FC combination induces significant ICD in tumor cell lines (Fig. 3), which can trigger the release of DAMPs and promote tumor antigen presentation, thereby activating the tumor immune microenvironment[28], we therefore evaluated the tumor immune microenvironment following treatment. Tumor tissues were collected 24 hours after the final treatment cycle (Fig. 5A) and analyzed for ICD marker. Consistent with the *in vitro* findings, immunohistochemical analysis revealed

markedly enhanced expression of the ICD marker HSP90 in the dTF-FCU1/5-FC-treated group (brown staining, Fig. 5B).

We also assessed the immune cells in tumor tissues collected 24 hours after the final treatment cycle (Fig. 5A). The results showed that the ratios of $CD3^+$ and $CD8^+$ T cells were significantly increased in the dTF-FCU1/5-FC treated tumors (Fig. 5D-5F), this finding was corroborated by immunofluorescence staining for CD8 (Fig. 5C). In contrast, the ratio of $CD4^+$ T cells decreased (Fig. 5D, 5G), especially the $CD4^+FoxP3^+$ regulatory T cell (Treg) subset (Fig. 5D, 5H). Besides, dTF-FCU1/5-FC treatment increased the percentages of granzyme B $(GZMB)^+$ $CD8^+$, TNF^+ $CD8^+$, TNF^+ $CD4^+$ T, and $GZMB^+$ $CD4^+$ T cells (Fig. 5M-5P), which indicates a robust activation of the T cell immune response in TME.

Next, T cell activation in the spleen was evaluated (Fig. 5A, Figure S4A). Following ex vivo stimulation of splenocytes with the LLC antigen, TNF-α production was significantly increased in both $CD8^+$ and $CD4^+$ T cells from mice treated with dTF-FCU1/5-FC (Figure S4B and S4C). Moreover, the combination therapy led to significantly higher frequencies of $GZMB^+CD8^+$ and $GZMB^+CD4^+$ T cells compared with dTF-FCU1 alone (Figure S4D and S4E). These data indicate that dTF-FCU1/5-FC combination promotes the activation of functional $CD8^+$ and $CD4^+$ T cells and enhances systemic antitumor immunity.

Given that the immunosuppressive TME plays a pivotal role in tumor progression and drug resistance[29,30], we next evaluated the effect of dTF-FCU1/5-FC treatment on immunosuppressive cell populations within tumor tissues. In addition to the reduction in Tregs described above, treatment also decreased the frequency of exhausted T cells ($PD\text{-}1^+TIM\text{-}3^+$) (Fig. 5D and 5I). Furthermore, M2-type tumor-associated macrophages (TAMs), which contribute to tumor growth, invasion, metastasis, and drug resistance, were moderately reduced following dTF-FCU1/5-FC treatment (Fig. 5D, 5J-5L).

In conclusion, these results demonstrate that the dTF-FCU1/5-FC combination therapy enhances antitumor immunity by activating $CD8^+$ and $CD4^+$ T cells while alleviating immunosuppression *in vivo*.

Discussion

In this study, we engineered a recombinant oncolytic VACV, dTF-FCU1, by integrating the prodrug-converting enzyme FCU1 into the *J2R* locus and deleting the viral RRM2 gene *F4L*. This dual-deletion design substantially enhanced tumor selectivity. In combination with 5-FC, the dTF-FCU1/5-FC regimen induced significant ICD response and profoundly remodeled the systemic antitumor immune response.

These findings represent further improvement in the tumor-selectivity of oncolytic viruses. In previous studies, VACV-based oncolytic vectors commonly have the TK gene (*J2R*) deleted to reduce virulence while preserving their replication capacity in tumor cells[13,31,32]. However, *J2R*-deleted VACV still exhibits considerable replication levels in normal cells[4]. Likewise, dTK-FCU1 showed replication capacity comparable to that of the wild-type VACV in control cell line HSF. This may be attributed to the virally

encoded, other highly active thymidylate kinase which provides an alternative thymidine triphosphate synthesis pathway[33].

Building on the strategy of targeting nucleotide metabolism, we further deleted the genes encoding subunits of RR, a key enzyme in de novo DNA synthesis, to increase tumor selectivity. RR is a heterotetramer consisting of RRM1 and RRM2, and is highly expressed in tumor cells requiring active dNTPs metabolism. Johann Foloppe et al. reported a VACV deleted both *J2R* and *I4L*, which shows promising selectivity for hepatocellular carcinoma cells[4]. A VACV with deletion of *J2R* and *F4L* exhibited remarkable selectivity for bladder cancer cells[12]. We generated VACVs by either deleting *J2R* and *F4L* or deleting of *J2R* and *I4L*, and observed superior tumor selectivity for the J2R/F4L-deleted VACV in the dTK-FCU1 backbone (Fig. 1E, 2A), which supports the pivotal role of *F4L* in controlling viral replication in cancer cells with heightened dNTPs demand[10].

OVs are often armed with transgenes to boost killing efficacy. The 5-FC/FCU1 system is commonly used in this context, with its antitumor activity been extensively validated in preclinical models[4,7,34]. FCU1 converts 5-FC to 5-FU and subsequent FdUMP, FdUTP, and FUTP. These metabolites disrupt normal nucleic acid metabolism, activate the ATR/Chk1 and ATM pathways, and ultimately induce apoptosis[14–17,35,36]. dTF-FCU1 acts in concert with the prodrug 5-FC, harnessing both direct viral oncolysis and local drug-mediated cytotoxicity, thus producing a potent antitumor effect. Our study found that the combination of dTF-FCU1 and 5-FC induced marked DNA damage, triggered pronounced apoptosis, resulted in potent killing of A549 and LLC cells, and significantly suppressed tumor growth in nude mice.

Notably, beyond DNA damage and apoptosis, the combination of dTF-FCU1/5-FC induces robust ICD in cancer cell lines, evidenced by increased surface CRT expression and elevated levels of ATP, HMGB1, and HSP90 released into the supernatant in A549, LLC, HepG2 and Huh-7 cells. Additionally, tumor growth was significantly suppressed in immunocompetent mice. ICD plays a crucial role in enhancing the anti-tumor immune response, which is a key objective in cancer therapy[37]. Previous studies indicate that both oncolytic viruses and 5-FU can independently induce ICD. FUVAC induced potent ICD in lung (A549) and colon (CT26) carcinoma cells[38], while Dafeng Xu et al. discovered that 5-FU treatment triggered ICD in HCC cells[39].

Importantly, the ICD response induced by dTF-FCU1/5-FC contributes to a profound remodeling of the systemic antitumor immune response. Specifically, dTF-FCU1/5-FC therapy promotes the intratumoral infiltration and activation of cytotoxic $CD8^+$ T cells, including granzyme B^+ $CD8^+$ T cells and TNF^+ $CD8^+$ T cells, as well as TNF^+ $CD4^+$ T cells, while simultaneously reduced immunosuppressive cell populations, including Tregs, exhausted T cells, and M2-type macrophages. This represents a shift from an immunosuppressive microenvironment to a more immunostimulatory one.

In addition, the therapeutic benefits extend beyond the tumor site. The combination therapy dTF-FCU1/5-FC also promotes systemic immune activation, such as in the spleen, the activation of $CD8^+$ T and $CD4^+$ T cells was also observed.

Unexpectedly, this study also observed a reduction in intratumoral $CD4^+$ T cells, consistent with previous findings of the VV-FCU1 and FUVAC studies [8,38]. The decrease in $CD4^+$ T cells may be partially associated with the reduction in Tregs. Study showed that 5-FU treatment can significantly downregulate Treg levels and reverse T cell exhaustion[40,41].

This study suffers from certain limitations. Our study primarily utilized subcutaneous xenograft models, which do not fully recapitulate the tumor microenvironment of orthotopic lung cancers. The therapeutic efficacy and immune infiltration profiles of dTF-FCU1/5-FC may differ in lung cancer in situ models and will be investigated in future work. Additionally, we recognize that potential synergistic effects of dTF-FCU1/5-FC combined with immunotherapeutic strategies, such as anti-PD-1 or anti-CTLA-4 antibodies, were not explored here. Given the strong rationale for combining oncolytic virotherapy with immune checkpoint blockade, such combination strategies will be a key focus of our subsequent studies. Although dTF-FCU1/5-FC demonstrates promising efficacy and safety in mouse models, its safety profile in lung cancer patients requires further evaluation.

Conclusions

This study reports a highly selective oncolytic VACV, dTF-FCU1. Combination with 5-FC further enhances its oncolytic efficacy through inducing DNA damage and ICD and remodeling the tumor immune microenvironment by activating $CD8^+$ T cells while suppressing Tregs, exhausted T cells and M2-type macrophages. dTF-FCU1/5-FC therapy effectively activates antitumor immunity while suppresses key immunosuppressive mechanisms, offering a promising strategy for the treatment of advanced lung and liver carcinomas. Future work is warranted to evaluate the safety profile and translational potential of this regimen in clinical settings.

Declarations

Availability of data and materials

All data associated with this study are present in the paper or the supplementary material.

Funding

This study was supported by funds from the Prevention and Control of Emerging and Major Infectious Diseases-National Science and Technology Major Project (2026ZD01911100 and 2026ZD01911102), from the National Key R&D Program of China (2023YFC2307902), from the National Natural Science Foundation of China (82271802 and 32200718), from the Fundamental Research Funds for Central Universities, Chinese Academy of Medical Sciences & Peking Union Medical College (3332021092).

Author contributions

J.F., B.A, F.X. and F.G. conceived the project. L.W., Y.H. and S.M performed the experiments and prepared the manuscript. F.Z., Lingwa Wang, Z.G., J.W., Z.K., M.W., S.R., Yurong He, Y.S. and W.G. performed the data curation and formal analysis. All authors contributed to experimental design. L.W., Y.H. and F.G. composed the manuscript. All authors reviewed the manuscript and discussed the work.

Ethics approval

The experimental procedures involving mice were conducted in accordance with the guidelines of the BeiJing Huilin Zegu Biotechnology Co., LTD. Institutional Animal Care and Use Committee (Approval No. HLZG-DWLL-2024-0602-04). The ethics approvals of the mouse study are described in the Methods section.

Competing interests

The authors declare no competing interests.

Acknowledgements

Mice tumor dissociation was conducted at the Core Facilities and Service Centers, NIPB, CAMS&PUMC. We thank Yan Xiao and Li Li for expert assistance with experiments.

References

1. Santos Apolonio, J. *et al.* Oncolytic virus therapy in cancer: A current review. *World journal of virology* 10, 229–255 (2021). https://doi.org/10.5501/wjv.v10.i5.229
2. Kaufman, H. L., Kohlhapp, F. J. & Zloza, A. Oncolytic viruses: a new class of immunotherapy drugs. *Nature reviews. Drug discovery* 14, 642–662 (2015). https://doi.org/10.1038/nrd4663
3. Cousin, S. *et al.* Phase 2 trial of intravenous oncolytic virus JX-594 combined with low-dose cyclophosphamide in patients with advanced breast cancer. *Exp Hematol Oncol* 11, 104 (2022). https://doi.org/10.1186/s40164-022-00338-2
4. Foloppe, J. *et al.* The Enhanced Tumor Specificity of TG6002, an Armed Oncolytic Vaccinia Virus Deleted in Two Genes Involved in Nucleotide Metabolism. *Molecular therapy oncolytics* 14, 1–14 (2019). https://doi.org/10.1016/j.omto.2019.03.005
5. Aye, Y., Li, M., Long, M. J. & Weiss, R. S. Ribonucleotide reductase and cancer: biological mechanisms and targeted therapies. *Oncogene* 34, 2011–2021 (2015). https://doi.org/10.1038/onc.2014.155
6. McFadden, G. Poxvirus tropism. *Nat Rev Microbiol* 3, 201–213 (2005). https://doi.org/10.1038/nrmicro1099
7. Hwang, T. H. *et al.* A mechanistic proof-of-concept clinical trial with JX-594, a targeted multi-mechanistic oncolytic poxvirus, in patients with metastatic melanoma. *Mol Ther* 19, 1913–1922 (2011). https://doi.org/10.1038/mt.2011.132

8. Fend, L. *et al.* Oncolytic virotherapy with an armed vaccinia virus in an orthotopic model of renal carcinoma is associated with modification of the tumor microenvironment. *Oncoimmunology* 5, e1080414 (2016). https://doi.org/10.1080/2162402X.2015.1080414
9. Ward, P. S. & Thompson, C. B. Metabolic reprogramming: a cancer hallmark even warburg did not anticipate. *Cancer cell* 21, 297–308 (2012). https://doi.org/10.1016/j.ccr.2012.02.014
10. Gammon, D. B. *et al.* Vaccinia virus-encoded ribonucleotide reductase subunits are differentially required for replication and pathogenesis. *PLoS Pathog* 6, e1000984 (2010). https://doi.org/10.1371/journal.ppat.1000984
11. Hendricks, S. P. & Mathews, C. K. Allosteric regulation of vaccinia virus ribonucleotide reductase, analyzed by simultaneous monitoring of its four activities. *J Biol Chem* 273, 29512–29518 (1998). https://doi.org/10.1074/jbc.273.45.29512
12. Potts, K. G. *et al.* Deletion of F4L (ribonucleotide reductase) in vaccinia virus produces a selective oncolytic virus and promotes anti-tumor immunity with superior safety in bladder cancer models. *EMBO Mol Med* 9, 638–654 (2017). https://doi.org/10.15252/emmm.201607296
13. Erbs, P. *et al.* In vivo cancer gene therapy by adenovirus-mediated transfer of a bifunctional yeast cytosine deaminase/uracil phosphoribosyltransferase fusion gene. *Cancer Res* 60, 3813–3822 (2000).
14. Longley, D. B., Harkin, D. P. & Johnston, P. G. 5-fluorouracil: mechanisms of action and clinical strategies. *Nat Rev Cancer* 3, 330–338 (2003). https://doi.org/10.1038/nrc1074
15. Paulsen, R. D. & Cimprich, K. A. The ATR pathway: fine-tuning the fork. *DNA Repair (Amst)* 6, 953–966 (2007). https://doi.org/10.1016/j.dnarep.2007.02.015
16. Huehls, A. M. *et al.* Poly(ADP-Ribose) polymerase inhibition synergizes with 5-fluorodeoxyuridine but not 5-fluorouracil in ovarian cancer cells. *Cancer Res* 71, 4944–4954 (2011). https://doi.org/10.1158/0008-5472.CAN-11-0814
17. Flynn, R. L. & Zou, L. ATR: a master conductor of cellular responses to DNA replication stress. *Trends Biochem Sci* 36, 133–140 (2011). https://doi.org/10.1016/j.tibs.2010.09.005
18. Galluzzi, L., Guilbaud, E., Schmidt, D., Kroemer, G. & Marincola, F. M. Targeting immunogenic cell stress and death for cancer therapy. *Nature reviews. Drug discovery* 23, 445–460 (2024). https://doi.org/10.1038/s41573-024-00920-9
19. Palanivelu, L., Liu, C. H. & Lin, L. T. Immunogenic cell death: The cornerstone of oncolytic viro-immunotherapy. *Front Immunol* 13, 1038226 (2022). https://doi.org/10.3389/fimmu.2022.1038226
20. Singh, H. M. *et al.* MicroRNA-sensitive oncolytic measles virus for chemovirotherapy of pancreatic cancer. *Molecular therapy oncolytics* 21, 340–355 (2021). https://doi.org/10.1016/j.omto.2021.04.015
21. Niavarani, S. R., Lawson, C., Boudaud, M., Simard, C. & Tai, L. H. Oncolytic vesicular stomatitis virus-based cellular vaccine improves triple-negative breast cancer outcome by enhancing natural killer and CD8(+) T-cell functionality. *Journal for immunotherapy of cancer* 8 (2020). https://doi.org/10.1136/jitc-2019-000465

22. Teramoto, K., Ohshio, Y., Fujita, T., Hanaoka, J. & Kontani, K. Simultaneous activation of T helper function can augment the potency of dendritic cell-based cancer immunotherapy. *J Cancer Res Clin Oncol* 139, 861–870 (2013). https://doi.org/10.1007/s00432-013-1394-4
23. Mandelboim, O., Bar-Haim, E., Vadai, E., Fridkin, M. & Eisenbach, L. Identification of shared tumor-associated antigen peptides between two spontaneous lung carcinomas. *J Immunol* 159, 6030–6036 (1997).
24. Martin, C. K. *et al.* Vaccinia Virus Arrests and Shifts the Cell Cycle. *Viruses* 14 (2022). https://doi.org/10.3390/v14020431
25. Zhang, H. *et al.* Therapeutic targeting of cell death-immune crosstalk in cancer to rewire the tumor immune microenvironment. *Mol Cancer* 24, 277 (2025). https://doi.org/10.1186/s12943-025-02491-8
26. Kroemer, G., Montegut, L., Kepp, O. & Zitvogel, L. The danger theory of immunity revisited. *Nat Rev Immunol* 24, 912–928 (2024). https://doi.org/10.1038/s41577-024-01102-9
27. DePeaux, K. & Delgoffe, G. M. Integrating innate and adaptive immunity in oncolytic virus therapy. *Trends in cancer* (2023). https://doi.org/10.1016/j.trecan.2023.09.012
28. Filley, A. C. & Dey, M. Immune System, Friend or Foe of Oncolytic Virotherapy? *Frontiers in oncology* 7, 106 (2017). https://doi.org/10.3389/fonc.2017.00106
29. Hinshaw, D. C. & Shevde, L. A. The Tumor Microenvironment Innately Modulates Cancer Progression. *Cancer Res* 79, 4557–4566 (2019). https://doi.org/10.1158/0008-5472.can-18-3962
30. Wu, B., Zhang, B., Li, B., Wu, H. & Jiang, M. Cold and hot tumors: from molecular mechanisms to targeted therapy. *Signal Transduct Target Ther* 9, 274 (2024). https://doi.org/10.1038/s41392-024-01979-x
31. Kelly, E. & Russell, S. J. History of oncolytic viruses: genesis to genetic engineering. *Mol Ther* 15, 651–659 (2007). https://doi.org/10.1038/sj.mt.6300108
32. Kim, J. H. *et al.* Systemic armed oncolytic and immunologic therapy for cancer with JX-594, a targeted poxvirus expressing GM-CSF. *Mol Ther* 14, 361–370 (2006). https://doi.org/10.1016/j.ymthe.2006.05.008
33. Romain, S. *et al.* DNA-synthesizing enzymes in breast cancer (thymidine kinase, thymidylate synthase and thymidylate kinase): association with flow cytometric S-phase fraction and relative prognostic importance in node-negative premenopausal patients. *Int J Cancer* 95, 56–61 (2001). https://doi.org/10.1002/1097-0215(20010120)95:1%3C56::aid-ijc1010%3E3.0.co;2-3
34. Heinrich, B. *et al.* Immunogenicity of oncolytic vaccinia viruses JX-GFP and TG6002 in a human melanoma in vitro model: studying immunogenic cell death, dendritic cell maturation and interaction with cytotoxic T lymphocytes. *Onco Targets Ther* 10, 2389–2401 (2017). https://doi.org/10.2147/OTT.S126320
35. Geng, L., Huehls, A. M., Wagner, J. M., Huntoon, C. J. & Karnitz, L. M. Checkpoint signaling, base excision repair, and PARP promote survival of colon cancer cells treated with 5-fluorodeoxyuridine but not 5-fluorouracil. *PLoS One* 6, e28862 (2011). https://doi.org/10.1371/journal.pone.0028862

36. Lavin, M. F. & Kozlov, S. ATM activation and DNA damage response. *Cell Cycle* 6, 931–942 (2007). https://doi.org/10.4161/cc.6.8.4180
37. Green, D. R., Ferguson, T., Zitvogel, L. & Kroemer, G. Immunogenic and tolerogenic cell death. *Nat Rev Immunol* 9, 353–363 (2009). https://doi.org/10.1038/nri2545
38. Nakatake, M., Kuwano, N., Kaitsurumaru, E., Kurosaki, H. & Nakamura, T. Fusogenic oncolytic vaccinia virus enhances systemic antitumor immune response by modulating the tumor microenvironment. *Mol Ther* 29, 1782–1793 (2021). https://doi.org/10.1016/j.ymthe.2020.12.024
39. Xu, D. *et al.* MTIF2 impairs 5 fluorouracil-mediated immunogenic cell death in hepatocellular carcinoma in vivo: Molecular mechanisms and therapeutic significance. *Pharmacol Res* 163, 105265 (2021). https://doi.org/10.1016/j.phrs.2020.105265
40. Zhang, J. *et al.* Editorial: Enhancing T cell function: innovations in cancer immunotherapy. *Front Immunol* 16, 1615030 (2025). https://doi.org/10.3389/fimmu.2025.1615030
41. Limagne, E. *et al.* Accumulation of MDSC and Th17 Cells in Patients with Metastatic Colorectal Cancer Predicts the Efficacy of a FOLFOX-Bevacizumab Drug Treatment Regimen. *Cancer Res* 76, 5241–5252 (2016). https://doi.org/10.1158/0008-5472.CAN-15-3164

Figures

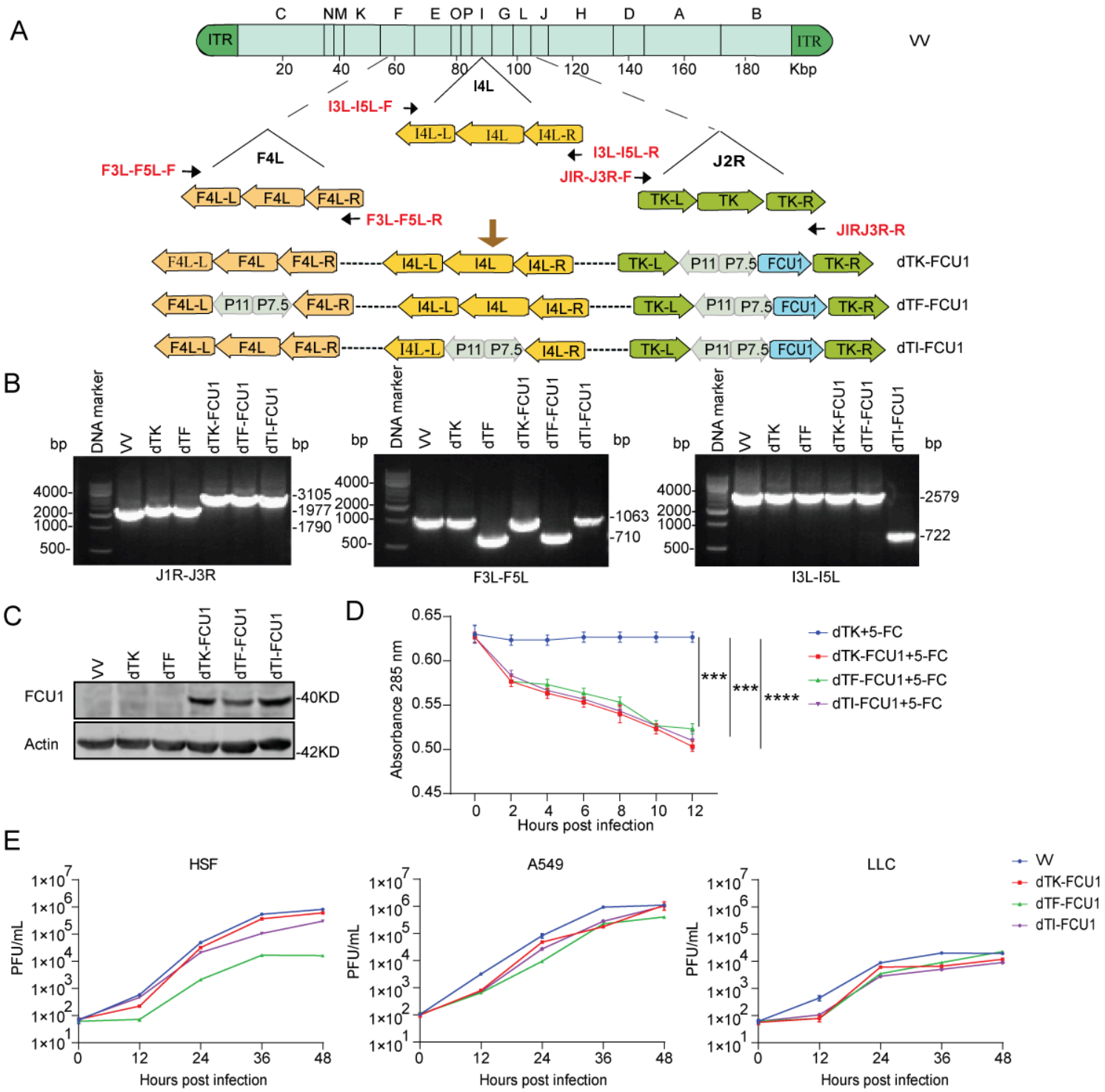


Figure 1

Generation and in vitro replication ability evaluation of recombinant VACV strains.

(A) Schematic representation of recombinant VACV strains used in this study. The dTK genome contains a deletion within the TK gene and is replaced by the vaccinia synthetic P11/P7.5 promoters. dTF contains deletions of both the TK and F4L genes. dTK-FCU1, dTF-FCU1, dTI-FCU1 contain in the TK locus the exogenous gene FCU1 under the control of the P7.5 promoter, the latter two simultaneously contain deletions in either the F4L or I4L gene. (B) Verification of the recombinant regions by PCR and nucleic

acid electrophoresis gel. PCR was performed on three recombinant regions (J1R-J3R, F3L-F5L, I3L-I5L) using the corresponding primers as shown in (A). Line 1 (left to right), 1Kb DNA ladder; Line 2-7, PCR products from the corresponding region (bottom). The arrows on the right indicates the presence of target bands with appropriate molecular weight. (C) Expression of FCU1 proteins in cells 24 h after infection by the recombinant VACVs at MOI=0.1. (D) Evaluation of FCU1 enzyme activity in infected cells. Spectrophotometric measurement of 5-FC turnover in Vero cells infected with recombinant VACVs (MOI=1). At indicated times post-infection, cell lysates were heat-inactivated and incubated with 5-FC (1.5 mM). Data are mean ± SD of three replicates. Two-way ANOVA. ***$p < 0.001$, ****$p < 0.0001$. (E) Growth curves for the indicated VACV strains in a normal human skin fibroblast line (HSF), a human lung cancer cell line (A549), and a mouse lung cancer cell line (LLC). The cells were infected with indicated VACV strains at MOI=0.005. The data depict the mean values ± SD of three separate experiments conducted independently.

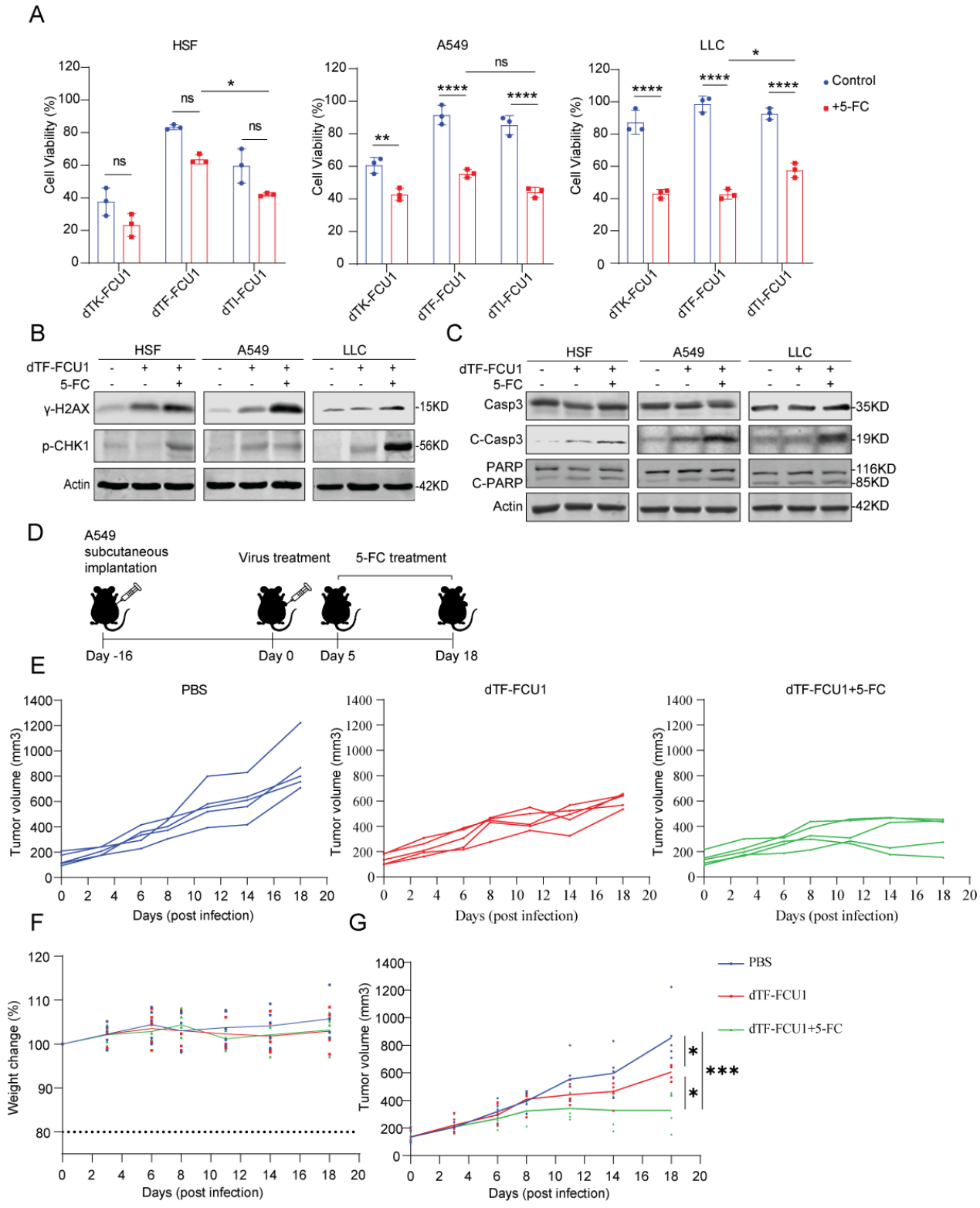


Figure 2

The combination of 5-FC and dTF-FCU1 induces significant damage to tumor cells.

(A) Evaluation of cytotoxicity from the combination of oncolytic viruses and prodrug activation. Cells were infected with indicated VACVs at MOI=0.001. 48 hours later, 5-FC at a final concentration of 1mM or an equal volume of 0.9% NaCl (control) was added. Cell viability was then evaluated 96 hours post-

infection using the CCK8 assay. Uninfected and 5-FC treated cells were used as control. Statistical analysis was performed with one-way ANOVA. Data are presented as mean ± SD of three replicates. *p < 0.05; **p < 0.01; ***p < 0.001; ****p < 0.0001; ns, not significant. (B-C) Assessment of double-stranded DNA damage (B) and apoptosis (C). Cells were infected with dTF-FCU1 at MOI=0.001. 48 hours post-infection, either 1mM 5-FC or an equal volume of 0.9% NaCl was added to the cell culture. Western blots were performed with cell lysates 48 h after drug treatment. Cells without virus and drug were Mock. Casp3, caspase3; C-Casp3, cleaved caspase3; C-PAPR, cleaved PARP. (D-F) The combined effects of dTF-FCU1 and 5-FC on tumor growth in nude mice subcutaneously implanted with A549. (D) Schematic diagram of treatment regimen. dTF-FCU1 was administered as a single intratumoral injection of 5×10^5 plaque-forming units (PFU), and oral 5-FC (twice daily) was initiated five days post-injection and continued for two weeks. (E) Tumor growth curves of A549 for individual mice in each group, PBS, dTF-FCU1 and dTF-FCU1/5-FC.(F) The changes in body weight. Dashed line represents the 80% level. The results are normalized against tumor-bearing mice without drug intervention (PBS). 5 mice in each group. (G) Evaluation of the growth of subcutaneously implanted A549 tumor size. Statistical analysis was performed with one-way ANOVA. 5 mice in each group. Mean ± SD was shown. *p < 0.05; ***p < 0.001

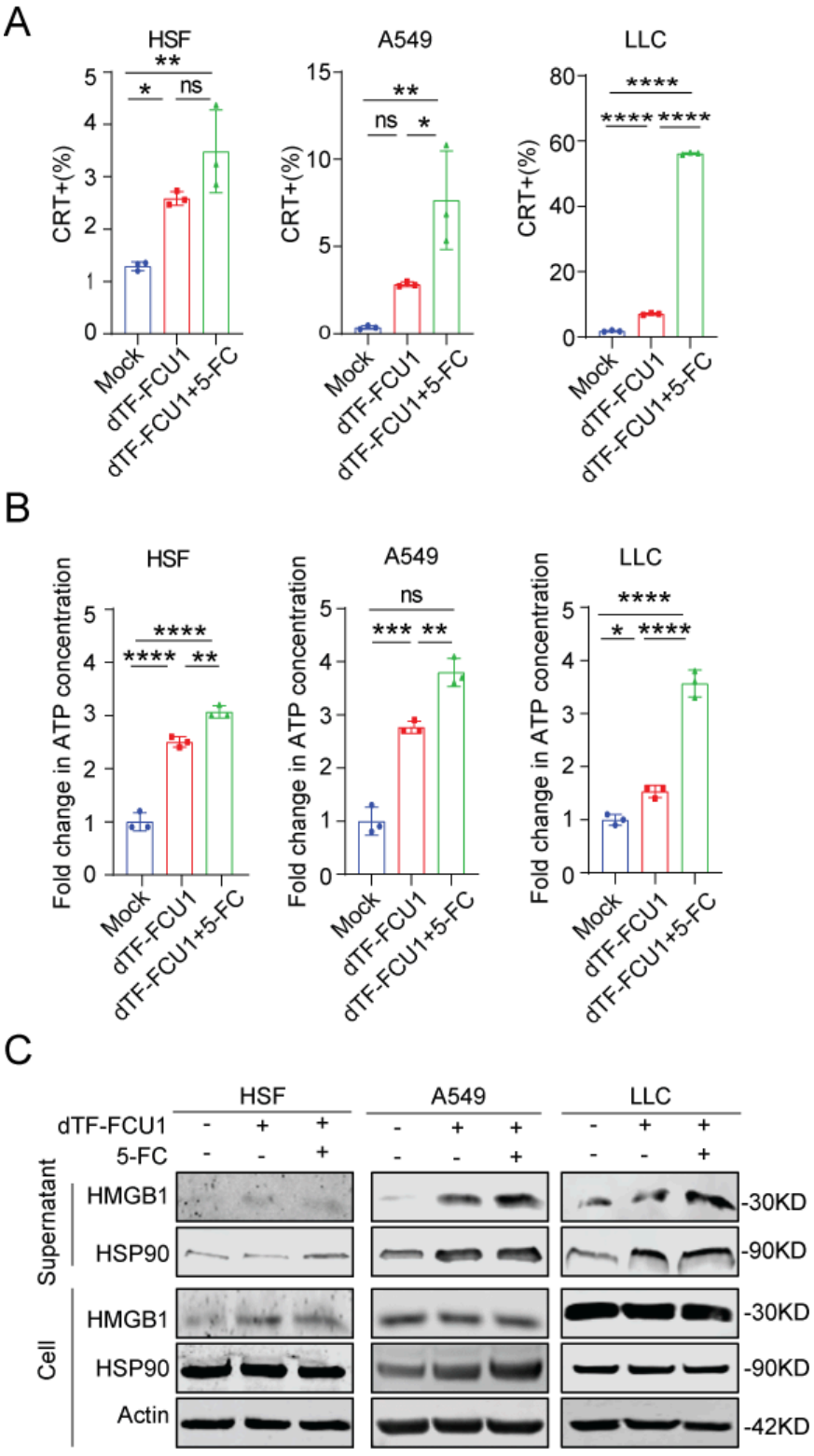
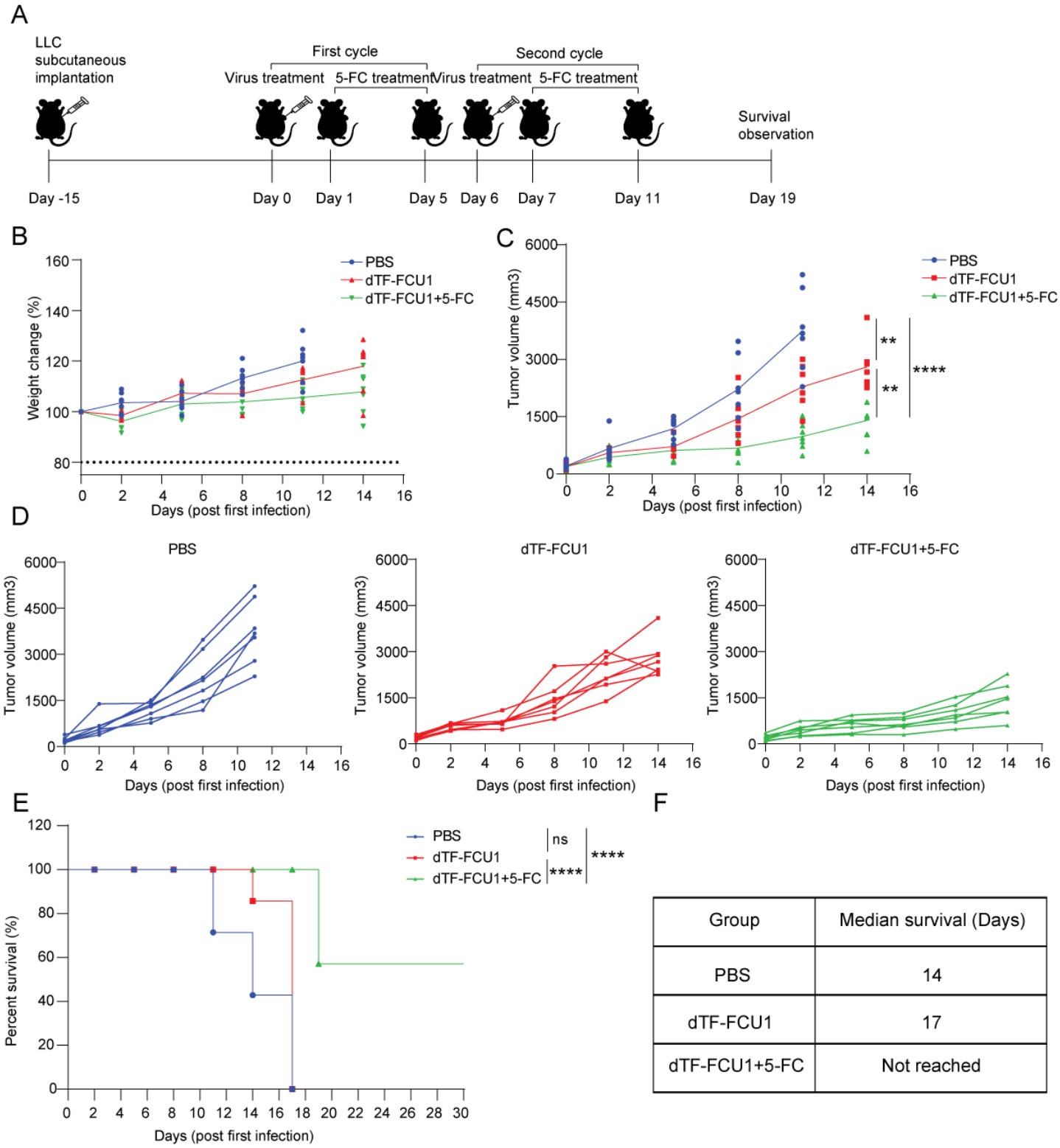


Figure 3

Detection of immunogenic cell death signals.

(A) The proportion of cells positive for CRT. Cells were infected with dTF-FCU1 at MOI=0.05. 2 hours post- infection, 5-FC (1mM) or 0.9% NaCl was added. 48 hours post-infection, cells were collected for Flow cytometry. Statistical analysis was performed with one-way ANOVA. (B) Relative ATP content in the

supernatant. Cells were infected with dTF-FCU1 (MOI=0.001). Two days post-infection, 1 mM 5-FC was added, supernatant was collected 48h treatment. ATP content was measured from the supernatant. Statistical analysis was performed with one-way ANOVA. (C) Western blots to detect ICD markers HSP90 and HMGB1 in cell lysis and culture supernatant infected with dTF-FCU1 with or without 5-FC treatment. Cell treatment and sample collection strategy were the same as in (B). The data represents the results of three replicates, shown as the mean ± SD. *p < 0.05; **p < 0.01; ***p < 0.001; ****p < 0.0001; ns, not significant.



Group	Median survival (Days)
PBS	14
dTF-FCU1	17
dTF-FCU1+5-FC	Not reached

Figure 4

Effect of dTF-FCU1 combined with 5-FC on immunocompetent mice bearing subcutaneous LLC tumors.

(A) Schematic diagram of treatment regimen. Two cycles of dTF-FCU1/5-FC treatment were administered, a single intratumoral injection of dTF-FCU1 (1×10^7 PFUs) was performed and 5-FC (or PBS) was given *per os* for 5 consecutive days starting on the next day after virus infection. At the end of the first 5-FC regimen, another same dose of dTF-FCU1 was injected into tumor sites and 5-FC was administered on the second day for 5 days. (B) The changes in body weight. Dashed line represents the 80% level. Values were shown as mean ± SD. 7 mice in each group. (C) Tumor size was measured in LLC-bearing immunocompetent mice. Measurements of tumor size within a group are stopped upon any death. Statistical analysis was performed with one-way ANOVA, shown as the mean ± SD. **p < 0.01; ****p < 0.0001. 7 mice in each group. (D) Tumor growth curves of LLC for individual mice in each group, PBS, dTF-FCU1 and dTF-FCU1/5-FC. (E) Survival curve was plotted for mice with subcutaneous LLC tumors. Statistical analysis was performed with Mantel-Cox test. ****p < 0.0001. (F) Median survival times for each group.

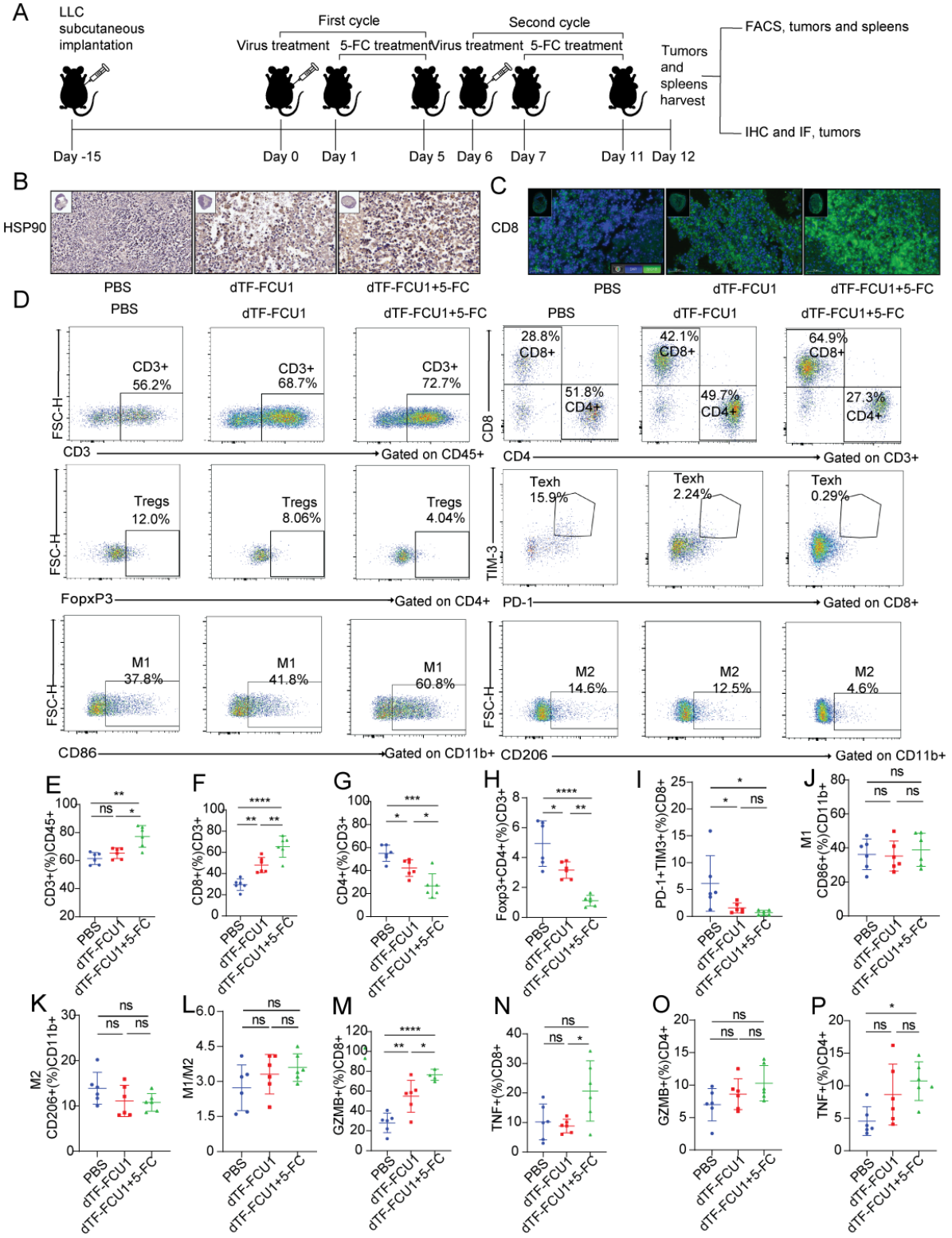


Figure 5

Alterations in the tumor immune microenvironment.

(A) Schematic diagram of treatment regimen. Tumor and spleen tissues were harvested 24 hours after the final administration of the two treatment cycles. 6 mice in each group. (B) Immunohistochemistry analysis of HSP90 (brown staining) in tumor tissues. (C) Immunofluorescence analysis of CD8 (green) in

tumor tissues. (D) Representative flow cytometry scatterplots for E-K. (E) The ratio of $CD3^+$T cells to leukocytes. Statistical analysis was performed with one-way ANOVA. (F-G) The ratio of $CD8^+$T cells (F) or $CD4^+$T cells (G) to $CD3^+$T cells. Statistical analysis was performed with one-way ANOVA. (H) The ratio of Treg cells to $CD3^+$ T cells. Statistical analysis was performed with one-way ANOVA. (I) The ratio of Texh cells to $CD8^+$ T cell. Statistical analysis was performed with one-way ANOVA. (J-L) Levels of M1 (J) and M2 (K) macrophages and ratios of M1 to M2 macrophages in tumor tissues (L). Statistical analysis was performed with one-way ANOVA. (M) The ratio of $CD8^+GZMB^+$T cells to $CD8^+$T cells. Statistical analysis was performed with one-way ANOVA. (N) The ratio of $CD8^+TNF^+$T cells to $CD8^+$T cells. Statistical analysis was performed with one-way ANOVA. (O) The ratio of $CD4^+GZMB^+$T cells to $CD4^+$T cells. Statistical analysis was performed with one-way ANOVA. (P) The ratio of $CD4^+TNF^+$T cells to $CD4^+$T cells. Statistical analysis was performed with one-way ANOVA. Data are presented as mean values ±SD. *p < 0.05; **p < 0.01; ***p < 0.001; ****p < 0.0001; ns, not significant.

Supplementary Files

This is a list of supplementary files associated with this preprint. Click to download.

- WBoriginaldata.pdf
- FCU1supplementaryinformation20260622TG.docx